Pergamon

PII: S1359-6454(96)00363-1

Acta mater. Vol. 45, No. 6, pp. 2435–2442, 1997

Published by Elsevier Science Ltd

1359-6454/97 $17.00 + 0.00

SHAPE OF A RHOMBOHEDRAL COHERENT $Ti_{11}Ni_{14}$ PRECIPITATE IN A CUBIC MATRIX AND ITS GROWTH AND DISSOLUTION DURING CONSTRAINED AGING

D. Y. LI and L. Q. CHEN

Department of Materials Science & Engineering, The Pennsylvania State University, University Park, PA 16802, U.S.A.

(Received 12 April 1996; accepted 19 September 1996)

Abstract—The shape of a coherent rhombohedral precipitate in a cubic matrix and its growth and dissolution during strain-constrained aging were investigated using a time-dependent Ginzburg–Landau kinetic model by taking into account the coupling between the constraint (applied) strain and the local strain. The effect of boundary conditions, constraint strain or constraint stress, has been discussed. A particular example of $Ti_{11}Ni_{14}$ precipitate growth in a TiNi shape memory alloy was considered without any a priori assumption about the particle shape. It was demonstrated that a $Ti_{11}Ni_{14}$ precipitate grown from a supersaturated cubic TiNi matrix has a lens-like shape, with its normal parallel to the $[111]_{B2}$ orientation of the matrix, in agreement with experimental observations. Precipitate growth and dissolution under various strain-constraint conditions have been discussed. © *1997 Acta Metallurgica Inc.*

INTRODUCTION

A coherent precipitate or a product phase has a number of variants which are oriented in different but equivalent crystallographic directions, if the precipitate or the product phase has a lower symmetry than the parent phase [1]. For example, the rhombohedral $Ti_{11}Ni_{14}$ precipitate in a cubic TiNi matrix has eight variants, whose $(111)_{Ti_{11}Ni_{14}}$ planes are, respectively, parallel to $\{111\}_{B2}$ of the matrix [2]. The eight variants fall into four groups and each group includes two variants which can be obtained mutually by a 180° rotation operation [e.g. $(111)_{Ti_{11}Ni_{14}} \| (111)_{B2}$ variant and $(111)_{Ti_{11}Ni_{14}} \| (\underline{111})_{B2}$ variant]. The variants usually have a non-spherical shape, since the lattice mismatch between the precipitate phase and the matrix is crystallographically anisotropic [3, 4]. During the precipitation process, different variants arrange in such a way that the strain energy caused by the variants is minimized. However, if an external strain or stress is applied during aging, an anisotropic distribution of precipitate variants could be attained and this may result in anisotropic properties of the material.

Equiatomic TiNi alloy is a well-known shape memory alloy [5–9]. It has a B2 structure (β phase) at ambient temperature and the β phase transforms to a monoclinic martensitic phase (M) at lower temperatures [10]. A workpiece made of martensitic TiNi alloy can be easily deformed through rearrangement of martensitic variants. The deformed TiNi piece can, however, restore its original shape by the reversible transformation $M \rightarrow \beta$. It was found that a TiNi alloy with 57.0–57.5 wt% Ni, aged under a constraint condition, exhibits an excellent two-way shape memory effect, called the all-round shape memory effect (ARSME) [11, 12]. Metallographic studies demonstrate that this ARSME is attributed to coherent $Ti_{11}Ni_{14}$ precipitates aligned in parallel, formed during the constrained aging. The reason is that a coherent $Ti_{11}Ni_{14}$ precipitate, having a near lens-like shape, brings an anisotropic strain field around it. If $Ti_{11}Ni_{14}$ precipitate variants are aligned in parallel, they could introduce a long-range internal stress field, which may control the "route" of the martensitic transformation, thus leading to the ARSME [11, 9]. If $Ti_{11}Ni_{14}$ precipitate variants are not in parallel, however, the local strain caused by differently oriented $Ti_{11}Ni_{14}$ variants may cancel each other out and no long-range internal stress field is attained.

The main objective of this research is to investigate the shape of rhombohedral precipitates coherently embedded in a cubic matrix and the effect of strain constraint on their growth and dissolution using numerical computer simulations. The shape of coherent precipitates has been studied by a number of researchers [13–21]. It is known that the shape of a coherent precipitate is determined by the balance between the interphase interfacial energy and the elastic strain energy. The strain energy, however, becomes more important with an increase in the precipitate size. Johnson and Cahn [13] demonstrated a change in morphology of a particle from a sphere to an ellipsoid with increasing particle size. Voorhees *et al.* [14] illustrated the temporal evolution of a circular particle and demonstrated the important role of the elastic strain energy in morphological evolution. Khachaturyan *et al.* [15] calculated the

elastic energy of a cubic precipitate as a function of its morphology and demonstrated the possibility of shape changes from sphere to doublet or octet of cubes. The transition of sphere to doublet or octet was also studied by McCormack *et al.* [16] and Doi [17]. Thompson *et al.* showed the morphological evolution of a precipitate with either a tetragonal or dilatational misfit in an elastically anisotropic medium with cubic symmetry [18]. Simulation studies were conducted by Wang, Chen and Khachaturyan [20, 21] to investigate the strain energy influence on the morphological evolution of cubic and tetragonal phases in a cubic matrix. Lee proposed a different approach, called the Discrete Atom Method, to analyse the effect of coherent strain energy on the morphological evolution of precipitate [19]. As mentioned earlier, the distribution of coherent precipitate variants is also important to materials' properties. An anisotropic variant distribution may lead to anisotropic behavior of the materials. The growth of a coherent precipitate could be strongly affected by external strains or stresses, and it may grow or shrink, depending on the interference of the applied strain or stress with the local strain. A particular case of the coarsening of precipitates in a cubic matrix, with dilatational mismatch strains, has been studied recently [22]. We employed spatially inhomogeneous continuous fields of concentration and structural order parameters to describe the rhombohedral precipitate morphology. The relaxation of these continuous fields is then determined by time-dependent Ginzburg–Landau (Allen–Cahn) [23, 24] and Cahn–Hilliard [25] equations taking into account the coupling between the constraint strain and the local strain. The emphasis will be on the shape of a single $Ti_{11}Ni_{14}$ precipitate and its growth or dissolution during constrained precipitation processes. The general case of microstructural evolution during precipitation of multi-particles under constraint conditions and their coarsening kinetics will be presented in another paper.

MODEL DESCRIPTION AND SIMULATION PROCEDURE

The growth of a $Ti_{11}Ni_{14}$ precipitate is driven by the difference in chemical free energies between the supersaturated TiNi matrix and the equilibrium TiNi matrix containing the $Ti_{11}Ni_{14}$ precipitate. In this work, we consider a single precipitate variant, and the "chemical" free energy is approximated using the Landau free energy polynomial

$$f(C,\eta)=\frac{A1}{2}(C-C_1)^2+\frac{A2}{2}(C-C_2)\eta^2-\frac{A3}{4}\eta^4+\frac{A4}{6}\eta^6 \qquad (1)$$

where, $C=C(\vec{r},t)$ is the concentration field which describes the compositional difference between the precipitate and matrix, and $\eta(\vec{r},t)$ the structural order parameter field which distinguishes the structural difference between the precipitate and matrix. If all variants of $Ti_{11}Ni_{14}$ precipitate are considered, four structural order parameters are required in the free energy model. The coefficients in equation (1) are chosen as follows: $A1=65.0$, $A2=7.54$, $A3=1.5$, $A4=1.45$ (the energies were measured in a unit, $mk_BT=7\times10^8$ ergs/cm^3, where $T=773$°C and m is a normalization coefficient). This choice provides the equilibrium compositions, C_1 (matrix) = 0.44 and C_2 (precipitate) = 0.38. By minimizing the chemical free energy with respect to η at a given C, one may obtain the relationship between C and the equilibrium structural order parameter, η_0. Consequently, the chemical free energy can be expressed as a function of the concentration only, i.e. $f(C,\eta)=f[C,\eta_0(C)]$. This function includes two branches: one corresponding to the TiNi matrix (β phase) and the other corresponding to the $Ti_{11}Ni_{14}$ precipitate phase. Figure 1 illustrates the chemical free energies as a function of C. It should be noted that the energy curves used here are only an approximation to the actual chemical free energies of the system. For the present simulation, the accuracy of the chemical free energy is not critical as long as it provides correct equilibrium compositions and the driving force for precipitation.

In addition to the chemical free energy, the interphase boundary energy also contributes to the system's total free energy. In this work, isotropic interfacial energy is assumed. The total free energy of an inhomogeneous system, in a stress-free state, may therefore be expressed as [21]

$$F_c=\int d^3r[\tfrac{1}{2}\alpha_1|\nabla C|^2+\tfrac{1}{2}\alpha_2|\nabla\eta|^2+f_c(C,\eta)] \qquad (2)$$

where α_1 and α_2 are gradient energy coefficients.

Another important contribution to the total free energy comes from the strain energy caused by the lattice mismatch between the $Ti_{11}Ni_{14}$ precipitate and the TiNi matrix. Equilibrium TiNi alloy has a B_2 structure (β phase: ordered b.c.c. structure, $a_0=3.01$ Å) [10], while $Ti_{11}Ni_{14}$ precipitate phase has

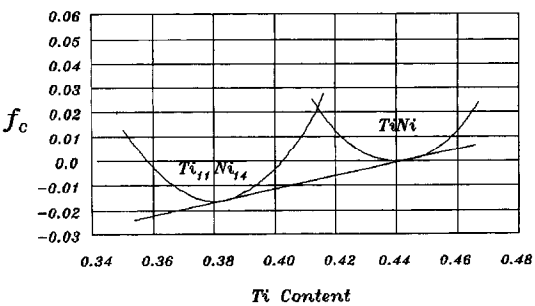

Fig. 1. Specific free energy vs concentration curves for β and $Ti_{11}Ni_{14}$ phases, calculated using equation (1) with $A1=65.0$, $A2=7.54$, $A3=1.5$, $A4=1.45$.

a rhombohedral structure ($a_0 = 6.72$ Å, $\gamma = 113.9°$) [2]. The lattice mismatch between these two phases influences the morphology of the $Ti_{11}Ni_{14}$ precipitate. The morphology (shape and orientation) of a coherent precipitate variant is then determined by competition between the strain energy and interphase boundary energy.

Calculation of the strain energy of a coherent precipitate was pioneered by Eshelby [27, 28], who derived equations of elastic strain of an ellipsoidal inclusion in an isotropic matrix based on the assumption that both phases have the same elastic moduli. Since then, Eshelby's theory has been modified, extended, and developed by many researchers [29–34]. An extension of Eshelby's theory was made by Lee *et al.* [33], who calculated the anisotropic elastic strain energy of coherent ellipsoidal precipitates in anisotropic solids. A general theory of strain energy of a coherent two-phase system with arbitrary morphology was proposed by Khachaturyan [3]. The crystal lattice mismatch between two phases, which is the source of the intrinsic elastic strain, is described by a stress-free strain or transformation strain, ϵ^0_{ij}. According to Khachaturyan [3], the strain field, $\epsilon_{ij}(\vec{r})$, of a two-phase system may be represented as the sum of the homogeneous and heterogeneous strains:

$$\epsilon_{ij}(\vec{r}) = \bar{\epsilon}_{ij} + \delta\epsilon_{ij}(\vec{r}) \tag{3}$$

where the homogeneous strain, $\bar{\epsilon}_{ij}$, is defined so that

$$\int_V \delta\epsilon_{ij}(\vec{r})\, \mathrm{d}^3r = 0. \tag{4}$$

The homogeneous strain is the uniform macroscopic strain, and the heterogeneous strain is chosen such that it has no macroscopic effects. In the case of homogeneous modulus (i.e. the elastic modulus of the second phase is the same as that of the matrix), the total elastic strain energy of a coherent mixture is expressed as [3, 26]

$$E_{\mathrm{el}} = \frac{V}{2} C_{ijkl}\, \bar{\epsilon}_{ij}\, \bar{\epsilon}_{kl} - V_{\mathrm{p}}\, C_{ijkl}\, \bar{\epsilon}_{ij}\, \epsilon^0_{kl} + \frac{V_{\mathrm{p}}}{2} C_{ijkl}\, \epsilon^0_{ij}\, \epsilon^0_{kl}$$

$$- \frac{1}{2} \int \frac{\mathrm{d}^3k}{(2\pi)^3} [n_i\, \sigma^0_{ij}\, \Omega_{jk}\, (\vec{n})\, \sigma^0_{kl}\, n_l] |\theta(\vec{k})|^2 \tag{5}$$

where V_{p} and V are the volume of the precipitate and total volume of the system, respectively. C_{ijkl} is the elastic constant, and $\sigma^0_{ij} = C_{ijkl}\epsilon^0_{kl}$. $\vec{n} = \vec{k}/k$ is a unit vector in the reciprocal space and n_i is the ith component of $\vec{n}$. $\Omega_{jk}(\vec{n})$ is a Green function matrix reciprocal to $\Omega^{-1}_{jk}(\vec{n}) = n_i C_{ijkl} n_l$. $\theta(\vec{k})$ is the Fourier transform of the so-called shape function $\theta(\vec{r})$:

$$\theta(\vec{k}) = \int \theta(\vec{r}) e^{-i\vec{k}\cdot\vec{r}} \mathrm{d}^3r. \tag{6}$$

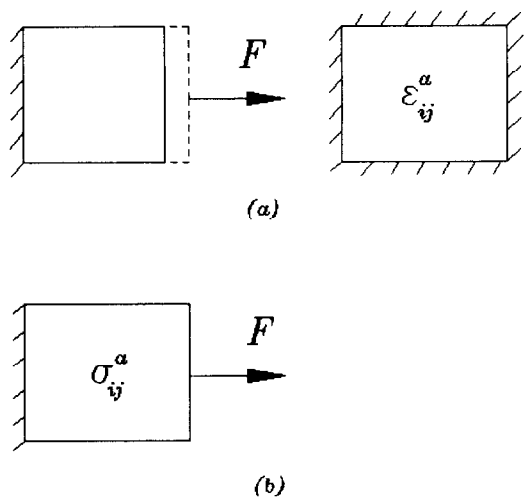

Fig. 2. Schematic illustration of two types of constraint: (a) strain-constraint: a body is elastically deformed by an applied force F, and the body boundary is then fixed so that a constant strain (applied), ϵ^a_{ij}, is established in the body; (b) stress-constraint: a constant force F is applied to a body without fixing the body boundary, thus resulting in a constraint stress (applied), σ^a_{ij}, in the body.

In the above integration, the singular branching point $k = 0$ is excluded. The shape function, $\theta(\vec{r})$, describes the shape of a precipitate; its value equal to unity within the precipitate and zero outside the precipitate. $\theta(\vec{r})$ may be represented by the structural order parameter: $\theta(\vec{r}) = \eta^2(\vec{r})/\eta^2_0$.

When the precipitation process (i.e. aging) is constrained, the strain field caused by a precipitate is, however, changed by the constraint strain or stress, and this results in a variation of the strain energy barrier to the growth of a precipitate. There are two types of constraint (Fig. 2). One is called *strain-constraint*, in which the system's boundary is fixed after applying an external force to the system, followed by the precipitation process. Under such a condition, the system is subjected to a constant external strain. The second type of constraint, called *stress-constraint*, is to apply a constant force on the system without fixing the system's boundary. Under this condition, the system is subjected to a constant external force. In the first case, the system is a mechanically isolated system but connected to a thermal reservoir which controls the system's temperature. This system is under an external strain, ϵ^a_{ij}. Since the boundary of the system is fixed, the homogeneous strain is the applied strain, i.e. $\bar{\epsilon}_{ij} = \epsilon^a_{ij}$. The total elastic strain energy is therefore given as

$$E'_{\mathrm{el}} = \frac{V}{2} C_{ijkl}\, \epsilon^a_{ij}\, \epsilon^a_{kl} + \frac{V_{\mathrm{p}}}{2} C_{ijkl}\, \epsilon^0_{ij}\, \epsilon^0_{kl} - \frac{1}{2} \int \frac{\mathrm{d}^3k}{(2\pi)^3}$$

$$[n_i \sigma^0_{ij}\, \Omega_{ik}\, (\vec{n})\, \sigma^0_{kl}\, n_l] |\theta(\vec{k})|^2 - V_{\mathrm{p}} C_{ijkl} \epsilon^a_{ij} \epsilon^0_{kl}. \tag{7}$$

The last term in equation (7) represents the coupling between the external strain and the strain caused by the precipitate. The governing potential of this system is the Helmholtz free energy, which includes the strain energy and the free energy F_c in the stress-free conditions given by equation (2), that is

$$F = F_c + E_{el}^{\epsilon}. \tag{8}$$

For the second type of constraint, a constant surface force is applied to the system during the precipitation process. This force makes the system become one which is connected with a mechanical reservoir that controls the external force, and also connected with a thermal reservoir which controls the system's temperature. In this case, the governing potential is the Gibbs free energy. The potential energy of such a system subjected to surface force $\vec{T}$ is expressed as

$$G = F_c + E_{el} - \int_S T_i \bar{u}_i \, ds \tag{9}$$

where $\bar{u}_i$ is the homogeneous strain. $T_i = \sigma_{ij}^a m_j$ and m_j is the exterior unit vector normal to S, the surface of the system. E_{el} is the elastic energy of the system given by equation (5). Since $\sigma_{ij,j}^a = 0$, by integrating $\int_V \sigma_{ij}^a \bar{u}_{i,j} \, dv = \int_S \sigma_{ij}^a \bar{u}_i m_j \, ds - \int_V \sigma_{ij,j}^a \bar{u}_i \, dv$ by parts we can calculate the third term in equation (9)

$$\int_S T_i \bar{u}_i \, ds = \int_S \sigma_{ij}^a m_j \bar{u}_i \, ds = \int_V \sigma_{ij}^a \bar{u}_{i,j} dv + \int_V \sigma_{ij,j}^a \bar{u}_i \, dv$$

$$= \int_V \sigma_{ij}^a \bar{u}_{i,j} \, dv = V \sigma_{ij}^a \bar{\epsilon}_{ij}. \tag{10}$$

Equation (9) can therefore be rewritten as

$$G = F_c + E_{el} - \int_S T_i \bar{u}_i \, ds = F_c + E_{el}$$

$$- V \sigma_{ij}^a \bar{\epsilon}_{ij} = F_c + E \tag{11}$$

where $E = E_{el} - V \sigma_{ij}^a \bar{\epsilon}_{ij}$. Minimizing E with respect to $\bar{\epsilon}_{ij}$

$$\frac{\partial E}{\partial \bar{\epsilon}_{ij}} = 0 = V C_{ijkl} \bar{\epsilon}_{ij} - V_p C_{ijkl} \epsilon_{kl}^0 - V \sigma_{ij}^a. \tag{12}$$

We obtain

$$\bar{\epsilon}_{ij} = S_{ijkl} \sigma_{kl}^a + \omega \epsilon_{ij}^0 \tag{13}$$

where S_{ijkl} is the compliance tensor and $\omega = V_p / V$. Substituting equation (13) back into the expression of E, we obtain the expression of E

$$E = \frac{V_p(1-\omega)}{2} C_{ijkl} \epsilon_{ij}^0 \epsilon_{kl}^0 - \frac{V}{2} S_{ijkl} \sigma_{ij}^a \sigma_{kl}^a - \frac{1}{2} \int \frac{d^3k}{(2\pi)^3}$$

$$[n_i \sigma_{ij}^0 \Omega_{jk}(\vec{n}) \sigma_{kl}^0 n_l] |\theta(\vec{k})|^2 - V_p \sigma_{ij}^a \epsilon_{kl}^0. \tag{14}$$

The growth of a $Ti_{11}Ni_{14}$ precipitate variant is simulated by the temporal evolution of the concentration and the structural order parameter fields whose relaxation is described by so-called time-dependent Ginzburg–Landau (TDGL) equations [20, 21]:

$$\frac{dC(\vec{r}, t)}{dt} = M \nabla^2 \frac{\delta F}{\delta C(\vec{r}, t)}$$

$$\frac{d\eta(\vec{r}, t)}{dt} = -L \frac{\delta F}{\delta \eta(\vec{r}, t)} \tag{15}$$

where M and L are kinetic coefficients which characterize the atomic diffusivity and interface boundary mobility. F is the total free energy of the system which includes the free energy in stress-free condition and the elastic strain energy. The expression for F is dependent on the constraint condition. In the strain-constant condition, F is the Helmholtz free energy [equation (8)], whereas in the stress-constraint condition, F is the Gibbs free energy [equation (11)]. In the present simulation, the strain-constraint condition is considered. The Helmholtz free energy is therefore used as the total free energy.

The TDGL equations were solved numerically in the reciprocal space. In order to save computing time, the simulation was conducted in a two-dimensional space (2D), which can be viewed as a projection of the 3D space. A 200×200 square grid was used to represent the system.

We chose the coordinate frame whose x, y, z axes are respectively parallel to $[1\bar{1}0]_{B2}$, $[11\bar{2}]_{B2}$, and $[111]_{B2}$ of the TiNi (B2) lattice. This coordinate frame may be called the variant coordinate frame. In this coordinate frame, the eigen-strain matrix of $Ti_{11}Ni_{14}$ precipitate is

$$(\epsilon_{ij}^{\circ}) = \begin{pmatrix} 0.014 & 0 & 0 \\ 0 & 0.014 & 0 \\ 0 & 0 & -0.029 \end{pmatrix}. \tag{16}$$

The elastic constants of the TiNi matrix and the $Ti_{11}Ni_{14}$ precipitate phase were assumed to be the same, and have the following values: $C_{11} = 1.62 \times 10^{11}$ Pa, $C_{12} = 1.29 \times 10^{11}$ Pa, and $C_{44} = 0.34 \times 10^{11}$ Pa [35]. Since the given elastic constants are valid only in the coordinate frame (x'–y'–z') whose three axes are, respectively, parallel to $[100]_{B2}$, $[010]_{B2}$, and $[001]_{B2}$, the elastic constants were converted to the variant coordinate frame (x–y–z) through the tensor transformation law [36]:

$$C_{ijkl} = S_{ii'} S_{jj'} S_{kk'} S_{ll'} C_{i'j'k'l'} \tag{17}$$

where $S_{ii'}$ is the coordinate transformation matrix which relates the x'–y'–z' coordinate frame to the x–y–z coordinate frame.

The gradient coefficients α_1 and α_2 were assumed to be 5.0; L and M are chosen to be 2.0. Reduced time t^* was used in the simulation, which is defined as $t^* = t/t_0$, and $t_0 = (Lk_BT)^{-1}$. The simulation was

performed in the following way. Initially, a spherical $Ti_{11}Ni_{14}$ particle with a radius $r_0 = 10\,\Delta r$ (where Δr is the length of a unit cell of the grid) was generated in a TiNi matrix. The matrix had a concentration $C_m = 0.43$ and its structural parameter $\eta = 0$. The concentration of the $Ti_{11}Ni_{14}$ particle was $C_2 = 0.38$ and its structural parameter had the equilibrium value $\eta = \eta_o = 1.02$. In order to investigate the constraint effect on the growth of the $Ti_{11}Ni_{14}$ particle, compressive and tensile stresses (equal to $\mp$ 30 MPa) were, respectively applied to the system initially and then fixed to the system's boundary. Compressive and tensile constraint strains were then, respectively, established for the entire process of the precipitate growth. These stresses were initially applied in the x–z plane and then at angles of 90°, 65°, 20°, and 0° to the z axis (i.e. $[111]_{B2}$ axis).

RESULTS AND DISCUSSION

The growth of a $Ti_{11}Ni_{14}$ precipitate in a supersaturated TiNi matrix without the strain constraint was simulated first. Figure 2 illustrates the growth of the precipitate viewed at the cross-section whose x (horizontal) and z (vertical) axes are parallel to $[1\bar{1}0]_{B2}$ and $[111]_{B2}$, respectively. The simulation time was chosen long enough for the final precipitate to approach its equilibrium shape. The simulation demonstrated that during the precipitation process the precipitate grew and its shape changed from an initial sphere to a lens-like plate with a bamboo leaf-like cross-section; the normal of the lens-like precipitate is parallel to the z axis, i.e. parallel to the $[111]_{B_2}$ direction. These simulation results agree with experimental observation [2, 11].

The morphology of a coherent precipitate is determined by both the elastic strain energy and the interphase interfacial energy. When the precipitate is small, the effect of the interfacial energy is predominant. As the precipitate grows, however, the effect of the strain energy becomes more important, because the ratio of the interfacial energy to the strain energy, i.e. $\xi = E_s/E_{el}$, decreases with increase in the length dimension of the precipitate. The interphase interfacial energy between a precipitate and the matrix can be calculated from

$$E_s = \int_V \mathrm{d}^3 r \{[f_c(C, \eta) + \tfrac{1}{2}\alpha_1 |\nabla C|^2 + \tfrac{1}{2}\alpha_2 |\nabla \eta|^2] - [f_\alpha \omega_p + (1 - \omega_p) f_\beta]\} \qquad (18)$$

where f_α and f_β are the chemical free energies of the $Ti_{11}Ni_{14}$ and TiNi phases, respectively, and ω_p is the volume fraction of the precipitate. For a simulated $Ti_{11}Ni_{14}$ precipitate as illustrated in Fig. 3, corresponding ξ values were calculated and they are 0.73 [corresponding to (b)] and 0.61 [corresponding to (c) and (d)], respectively. For a realistic $Ti_{11}Ni_{14}$

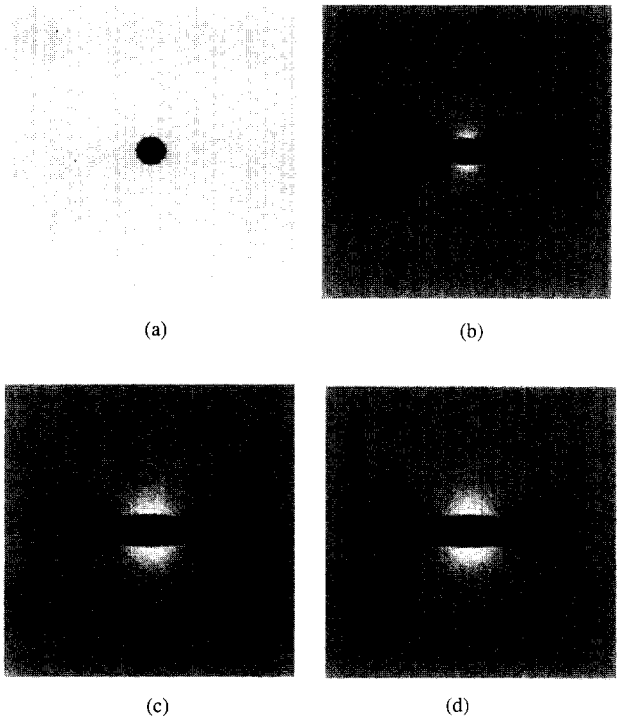

Fig. 3. Growth of a $Ti_{11}Ni_{14}$ variant, viewed at the cross-section; the normal of the lens-like precipitate is parallel to the $[111]_{B2}$ direction: (a) $t^* = 0$, (b) $t^* = 1.0 \times 10^3$, (c) $t^* = 3.5 \times 10^3$, (d) $t^* = 6.1 \times 10^3$.

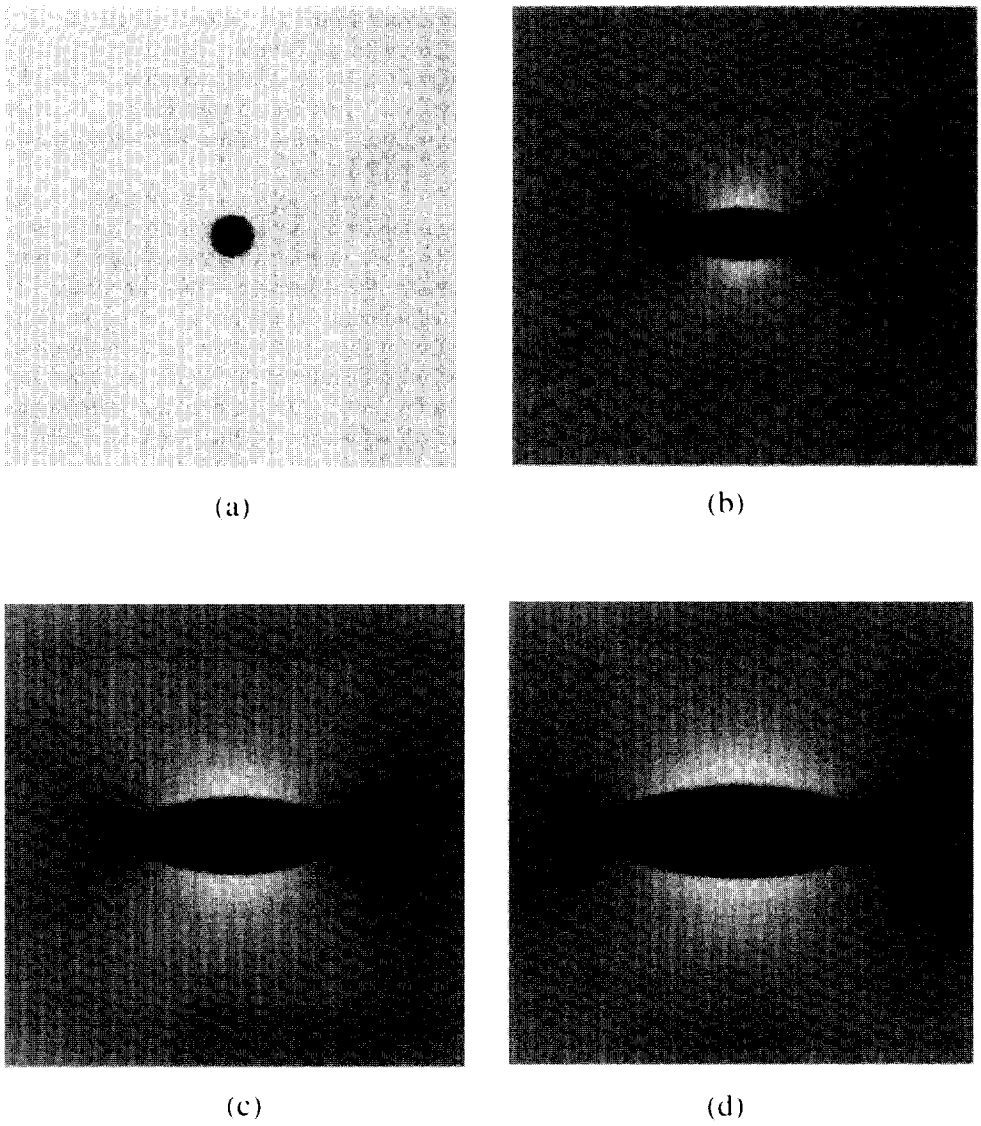

Fig. 4. Growth of a $Ti_{11}Ni_{14}$ particle under a compressive constraint strain, applied along the normal to the lens-like variant; the constraint strain was established by an initially applied stress which was equal to -30 MPa: (a) $t^* = 0$, (b) $t^* = 1.0 \times 10^3$, (c) $t^* = 2.1 \times 10^3$, (d) $t^* = 3.5 \times 10^3$.

precipitate, its strain energy could be estimated using the approximation: $E_{el} = \lambda \epsilon^2 V_p$ (λ and ϵ are the typical elastic modulus (10^{11} Pa) and typical stress-free transformation strain (10^{-2}), respectively, and V_p is the volume of the precipitate); the interfacial energy of the precipitate can be calculated using $E_s = \gamma_s S_p$ (γ_s and S_p are the specific interfacial energy and the surface area of the precipitate, respectively). A lens-like $Ti_{11}Ni_{14}$ precipitate with a diameter of 0.1 μm and thickness 0.05 μm has an approximate volume of 1×10^{-3} μm^3 and a surface area of 6×10^{-2} μm^2. Since the interfacial energy of coherent precipitates is generally on the order of 10^2 erg/cm^2, the interfacial energy of such a $Ti_{11}Ni_{14}$ precipitate is therefore on the order of 6×10^{-8} ergs; the strain energy of the precipitate is on the order of $E_{el} = \lambda \epsilon^2 V_p \approx 1 \times 10^{-7}$ ergs. Thus the ratio, ξ, of the interfacial energy to the strain energy of the $Ti_{11}Ni_{14}$ precipitate is on the order of 10^{-1}, which matches the values of ξ obtained in the simulation. Therefore, the numerical coefficients employed in the simulation provide a reasonable value for the ratio of the interfacial energy to the elastic strain energy.

Effects of both tensile and compressive constraint strains on the precipitate growth were then investigated. Figure 4 illustrates the effect of a compressive constraint strain on the growth of a $Ti_{11}Ni_{14}$ precipitate. It was demonstrated that when the compressive constraint strain was parallel to the z axis (i.e. $[111]_{B_2}$, the normal to the $Ti_{11}Ni_{14}$ precipitate plate), the precipitate grew faster than that without the constraint. This positive effect of compressive constraint strain on the precipitate growth comes from the reduction in strain energy by the coupling

of the constraint strain with the local strain. This conclusion may also be drawn simply from the eigen-strain, from which one may see that the precipitate has a compressive strain component in the z direction but a lower tensile component in x–y plane. This implies that when a precipitate nucleus is formed and grows in the matrix, it could introduce a tensile strain in the z direction but a lower compressive strain in the x–y plane. This strain energy increases the system's free energy, and thus brings an energy barrier to the precipitate's growth. When a compressive constraint strain is applied in the z direction during the precipitation process, however, it reduces both the local tensile strain in the z direction and the compressive strain in the x–y plane. As a result, the strain energy caused by the precipitate is reduced, and this in turn favors the growth of the precipitate. A similar phenomenon was observed in other systems, e.g. the precipitation of disk-like α'' ($Fe_{16}N_2$) from a supersaturated Fe–N alloy. The α'' disk causes a compressive strain parallel to its normal, which is significantly larger than other strain components. When a tensile stress is applied parallel to the normal to this variant, nucleation and growth of the variant is greatly promoted, against others that are oriented in different crystallographic directions [37, 38].

The simulation also demonstrated that the effect of tensile constraint strain on the growth of $Ti_{11}Ni_{14}$ precipitate is opposite to that of a compressive constraint strain. This is because the tensile constraint strain, when applied along the z axis, enhances both the local tensile strain in the z direction and the compressive strain in the x–y plane, and therefore increases the local strain energy. As a result, the growth of the precipitate is retarded, and it may shrink and dissolve eventually.

When a stress was applied in different directions, however, the effect of the resultant constraint strain on the precipitate growth changed. In the case of a compressive constraint strain, as the direction of the strain deviates from the normal to a $Ti_{11}Ni_{14}$ plate (i.e. the z axis), the growth rate of the precipitate is decreased. This variation with change in the direction of the applying strain (or initially applied stress) is demonstrated in Fig. 5, which illustrates the growth of a precipitate under a compressive constraint strain applied at angles of 0°, 20°, and 65° to the normal of the precipitate. One may see that, as the applying direction of the compressive constraint strain approached the x axis, the effect of the constraint strain was reversed, and it retarded the growth of the precipitate. This reversed effect was so strong that it made the initially embedded $Ti_{11}Ni_{14}$ particle shrink, and even dissolve when the stress was applied along the x axis. This reversed effect occurred because, as the compressive constraint strain approached the x axis, it enhanced both the local compressive strain in the x–y plane and the tensile strain in the z direction. Consequently, the local strain energy was not reduced but increased by the applied compressive strain, and this retarded the growth of the precipitate.

If the applied strain is a tensile one, however, its effect on the growth of the precipitate is opposite to that of a compressive constraint strain. When applied in the z direction, the tensile strain retarded precipitate growth, but it favored precipitate growth as the applying direction of the strain approached the x axis.

CONCLUSION

In order to better understand the morphological evolution of $Ti_{11}Ni_{14}$ precipitate and its selective variant growth in TiNi shape memory alloys during constrained precipitation processes and to develop efficient processing routes to control the microstructure of $Ti_{11}Ni_{14}$–TiNi two-phase systems, computer simulation studies were conducted on the shape of a single coherent $Ti_{11}Ni_{14}$ precipitate variant and its

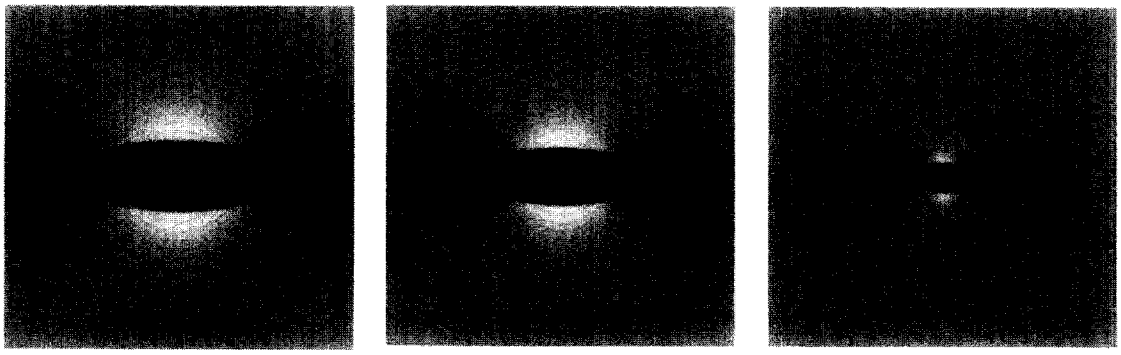

(a) (b) (c)

Fig. 5. Variation in effect of compressive strain on $Ti_{11}Ni_{14}$ variant growth with an increase in the angle between the normal to the variant and the direction of the applied strain: (a) 0°, (b) 20°, (c) 65°. The particle dissolved when the strain was applied at 90° to the normal of the variant (the constraint strain was established by the initially applied stress which was equal to −30 MPa); $t^* = 3.5 \times 10^3$.

growth under applied constraint strains, using a time-dependent Ginzburg–Landau kinetic model and taking into account the coupling between the applied constraint strain and the local strain caused by the precipitate. It was demonstrated that a $Ti_{11}Ni_{14}$ precipitate grown from supersaturated TiNi matrix has a lens-like shape, and its growth is strongly affected by the constraint strain applied during the precipitation process. The growth of a $Ti_{11}Ni_{14}$ precipitate variant may accelerate or the variant may shrink, depending on the interference between the applied strain and the local strain. The mechanism of precipitate growth, morphological evolution, and the constraint effects have been discussed.

Acknowledgements—The authors would like to thank Armen Khachaturyan for many useful discussions. This work is supported by the Office of Naval Research Young Investigator Program under grant number N-00014-95-1-0577 and calculations were performed at the Pittsburgh Supercomputing Center.

REFERENCES

1. Portier, R. and Gratias, D., *J. de Physique*, 1982, **43** (Colloque C4, suppl. 12), C4–17.
2. Nishida, M., Wayman, C. M., Kainuma, R. and Honma, T., *Scripta metall.*, 1986, **20,** 899.
3. Khachaturyan, A. G., *Theory of Structural Transformations in Solids*. John Wiley & Sons Inc., New York, 1983.
4. Porter, D. A. and Easterling, K. E., *Phase Transformations in Metals and Alloys*. Van Nostrand Reinhold Co., 1989.
5. Wayman, C. M., *Prog. Mater. Sci.*, 1992, **36,** 203.
6. Nagasawa, A., *Prog. Mater. Sci.*, 1971, **31,** 136.
7. Matsumoto, O., Miyazaki, S., Otsuka, K. and Tamura, H., *Acta metall.*, 1987, **35,** 2137.
8. Miyazaki, S. and Wayman, C. M., *Acta metall.*, 1988, **36,** 181.
9. Li, D. Y., Wu, X. F. and Ko, T., *Phil. Mag.*, 1991, **63,** 585.
10. Chandra, K. and Purdy, G. R., *J. appl. Phys.*, 1968, **39,** 2176.
11. Kainuma, R., Matsumoto, M. and Honma, T., *Proc. ICOMAT-86*, 1987, Japan Inst. of Metals, Aoba Aramaki, Sendai 980, Japan, p. 717.
12. Kaneko, K., Uehara, M., Aoki, H., Kubo, M., Suzuki, T. and Yoshida, A., *J. Soc. Mater. Sci., JPN*, 1993, **42,** 1103.
13. Johnson, W. C. and Cahn, J. W., *Acta metall.*, 1984, **32,** 1925.
14. Voorhess, P. W., McFadden, G. B. and Johnson, W. C., *Acta metall.*, 1992, **40,** 2979.
15. Khachaturyan, A. G., Semenovskaya, S. V. and Morris, J. W. Jr, *Acta metall.*, 1988, **36,** 1563.
16. McCormack, M., Khachaturyan, A. G. and Morris, J. W. Jr, *Acta metall. mater.*, 1992, **40,** 325.
17. Minoru Doi, *Mater. Trans., JIM*, 1992, **33,** 637.
18. Thompson, M. E., Su, C. S. and Voorhees, P. W., *Acta metall. mater.*, 1994, **42,** 2107.
19. Lee, J. K., *Scripta metall. mater.*, 1995, **32,** 559.
20. Wang, Y. and Khachaturyan, A. G., *Acta metall. mater.*, 1995, **43,** 1837.
21. Wang, Y., Wang, H., Chen, L. Q. and Khachaturyan, A. G., *J. Am. Ceram. Soc.*, 1993, **76,** 3029.
22. Hort, W. and Johnson, W. C., *Script. metall. mater.*, 1996, **34,** 1015.
23. Gunton, J. D., Miguel, M. S. and Sahni, P. S., in *Phase Transitions and Critical Phenomena*, Vol. 8, ed. C. Domb and J. L. Lebowitz. Academic Press, New York, 1983, pp. 267–466.
24. Allen, S. M. and Cahn, J. W., *Acta metall.*, 1979, **27,** 1085.
25. Cahn, J. W. and Hilliard, J. E., *J. Chem. Phys.*, 1958, **28,** 258.
26. Khachaturyan, A. G., Semenovskaya, S. and Tsakalaos, T., *Physical Review* 1995, **B52,** 1.
27. Eshelby, J. D., *Proc. R. Soc.*, 1957, **A241**, 376.
28. Eshelby, J. D., *Proc. R. Soc.*, 1959, **A252,** 561.
29. Walpole, L. J., *Proc. R. Soc.*, 1967, **A300,** 270.
30. Kinoshita, N. and Mura, T., *Phys. stat. solidi (a)*, 1971, **5,** 759.
31. Asaro, R. J. and Barnett, D. M., *J. Mech. Phys. Solids*, 1975, **23,** 77.
32. Mura, T., Mori, T. and Kato, M., *J. Mech. Phys. Solids*, 1976, **24,** 305.
33. Lee, J. K., Barnett, D. M. and Aaronson, H. I., *Metall. Trans.*, 1977, **8A,** 963.
34. Mori, T., Cheng, P. C., Kato, M. and Mura, T., *Acta metall.*, 1978, **26,** 1435.
35. Mercier, O., Melton, K. N., Gremaud, G. and Hägi, J., *J. appl. Phys.*, 1980, **51**(3), 1833.
36. Fedorov, F. I., *Theory of Elastic Waves in Crystals*. Plenum Press, New York, 1968.
37. Nakada, Y., Leslie, W. C. and Chray, T. P., *Trans. Am. Soc. Metals.*, 1967, **60,** 223.
38. Tanaka, Y., Sato, A. and Mori, T., *Acta metall.*, 1978, **26,** 529.